JOURNAL OF OPTOELECTRONICS AND ADVANCED MATERIALS Vol. 10, No. 10, October 2008, p. 2684 - 2693

Nanodesigning of SiO_2 powders obtained from silica sols by ultrasonic spray pyrolysis

V. JOKANOVIĆ*, B. JOKANOVIĆ[a]
Institute of Nuclear Sciences "Vinča", P.O. Box 522, 11001 Belgrade, Serbia
[b]*TU Clausthal, Institut fur Metallurgie, Department Termochemie und Mikrokinetik, Clausthal, Germany*

The mechanism of the synthesis of silicon dioxide particles by ultrasonic spraying of a silica sol as a precursor is the subject of this work. The structural design of the obtained particles was defined as an organized structure of basic motives, silica chains forming sol particles, sub-particles and finally up to the particle level. TGA analysis was employed to define the size of the silica chains in the sol particles. The mean particle size obtained by spray pyrolysis was 1.68 μm, with sub-particles of 25-30 nm. Based on the application of a suitable theoretical model, the mean particle diameter and sub-particle values were calculated as 1.8 μm and 38.4 nm, respectively. The theoretically and experimentally obtained values are in good agreement, confirming that advanced modeling of the silicon dioxide structure at the particle and sub-particle level is possible. The mean size of a sol particle obtained in the hydrothermal procedure was 7.5 nm and the size of the structural motive of the silica chain consisting of sol particles is built up from 18-20 tetrahedral cells of silicon dioxide.

(Received April 26, 2008; accepted August 14, 2008)

Keywords: Ultrasonic spray pyrolysis, Hydrothermal synthesis, Silica sol, Nanostructured design

1. Introduction

High performance silicon dioxide ceramics and glasses, due to their good optical transmittance, mechanical hardness, chemical durability, thermal stability, low temperature expansion coefficient, and high laser damage threshold, are extensively applied in the production of optoelectronic laser diodes, telecommunication optical fibers, medical laser delivery systems and military optical sensors [1-10].

As will be shown in this paper, the method of spray pyrolysis can be used for the synthesis of SiO_2 powder and is one of the most suitable methods for the production of spherical powders with a narrow size distribution. It was the favorite method in our previous investigations related to the synthesis of different systems/materials, such as Al_2O_3, mullite, cordierite, SiO_2, SiO_2 - rare-earth dopants, TiO_2, calcium hydroxyapatite, AgI and phosphorous doped tungsten bronzes [11-18]. In this paper, a theoretical model of structure and substructure design, previously verified for numerous ceramic systems and published in relation to them, is now applied to the SiO_2 system. [11-18].

This theoretical model presents a new approach to the explanation of the mechanism of formation of aerosol droplets by introducing a break-up mechanism of capillary waves formed on the meniscus surface of a precursor liquid [12-14, 17]. As it was shown in previous research, the main advantage of this method is related to its unique capability (compared to other well-known approaches, such as the Suslik, Lange and Peskin and Raco approaches [3, 19-21]) to give a detailed picture of the structure of a powder from the aspects of size and frequency of appearance of each individual particle and its substructure.

In addition to atomization, as the most important stage of spray pyrolysis, the process of precursor synthesis is important for creating the structure of the finally obtained particles. Hence, a hydrothermal method for the synthesis of a SiO_2 sol, as one of the most promising for the preparation of very preciously tailored precursors, is considered.

Designed SiO_2 precursors as nanomaterials and in their substructure sub-nanostructured materials, obtained in hydrothermal synthesis in the subsequent step of spray pyrolysis, enables precisely designed structures of silica particles at multi levels (from particles and sub-particles, to the level of nanosol particles and their constituents, silica chains and tetrahedrons) to be obtained. [11-14,17].

This can be realized by carefully choosing the thermal conditions of the spray pyrolysis process. As a consequence of the above-mentioned treatment, the so-obtained, completely multilevel designed SiO_2 systems might have high activity suitable for various applications.

This approach to the synthesis clearly supports the elements of molecular and nanoengineering, which may have substantial importance in future investigations of self-assembled systems. Such highly organized, multilevel structures possess a number of application potentials due to their diverse properties, such as optical activity and improved catalytic reactivity (high surface-to-volume ratio).

Finally some unique properties of the system on the low level of the structural organization (e.g. confined physical properties), may be retained in the process of enlargement of the sub-elements and their constituents into much bigger macro-assembles (macroblocks), showing the same unique characteristics on a much higher level of the organization (macrolevel). In spite of expansion of sub-

elements by their association, it is feasible to retain fully their individuality in a real organized structure by controlling their contacts (in each level of the structure hierarchy), on the level of dotted contacts to obtain blocks of the so-called activated structure [17].

2. Experimental

2.1 Sol and powder preparation

The silica sol was prepared by mixing a water glass solution ($Na_2O_x3SiO_2$ with the silicate module SiO_2/Na_2O ratio of 3.75 in de-ionized water) of viscosity 2.2 Pas with a 0.1N HCl solution. The soaking was accomplished by adding the 0.1N HCl solution dropwise to the water glass solution at 80 °C under intensive mixing with a magnetic stirrer. The total amount of added HCl corresponded to the stoichiometric ratio necessary to complete the neutralization reaction, i.e., hydrolysis of the given amount of water glass solution. In the starting mixture, the ratio of solid phase to the liquid phase was 1:4. After addition of the total amount of 0.1N HCl, the mixture was transferred into an autoclave and the soaking was continued for 5 h at a temperature of 120 °C under a pressure of 3 bars.

The so obtained silicon acid precipitate was then separated from the solution using an ultracentrifuge at 10.000 rotations per minute followed by the addition of de-ionized water in order to obtain a liquid to solid phase ratio of 4:1. In addition, a small amount of HCl (a fifth of the previously employed amount) was dripped into the solution. The mixture was transferred again into the autoclave for further treatment according under the previously given procedure. Finally, the silicon acid precipitate was separated from the liquid phase by ultracentrifugation and the supernatant was decanted.

In the second phase of the preparation, the silicon acid precipitate was transformed into a sol. This was achieved by taking 20 g of the silicon acid obtained by soaking using the above-described procedure and adding 200 ml of deionized water with the pH set to 10 (using a 0.1N NaOH solution). The system was then intensively mixed at 80 °C for 2 hours and its pH set again to 10 by the dropwise addition of a 0.1N NaOH solution. The mixture was transferred into an autoclave and further treated at a temperature of 120 °C under a pressure of 3 bar for 8 h. After completion of the hydrothermal treatment, the pH of the silicon acid sol was 9.

During the next procedure, the concentration of the obtained sol solution was set to the value of 2M silica and then subjected to ultrasonic spray pyrolysis. The pyrolysis conditions were: frequency of the ultrasonic atomizer, f = 1.7 MHz, working temperature in the tubular furnace, T = 1000 °C and a carrier gas – air – flow velocity, v = 0.011 m/s.

2.2 Characterization methods

The following characterization methods were used for the synthesized materials: transmission electron microscopy, TEM, (JOEL JEM 2000 FX), IR spectroscopy (PERKIN ELMER 983G) for phase analysis. Thermogravimetric and differential thermal analysis, TGA/DTA, (AMNICO) of the SiO_2 powder (obtained by drying the SiO_2 powder at 150 °C) was used to determine the structural motives of the SiO_2 sol particles, based on the determination of the water bound in them. The heating rates from room to the final temperature of 800 °C were 5 and 50 °C/min, respectively.

Light scattering was performed in the dynamical mode using a Light Scattering System BI-200SM, Brookhaven Instruments instrument, equipped with a BI-200SM goniometer, a BI-9000AT correlator, a temperature controller and a Cohereny INOVA 70C argon-ion laser. The dynamic light scattering measurements were performed using a laser excitation of 135 mW at 514.5 nm with a 90° detection angle. Particle size distributions were calculated using Brookhaven Instruments Particle Sizing software.

The morphology, size distribution, average size of silicon dioxide particles, and substructure were determined by scanning electron microscopy, SEM, (JEOL: JKSM-5300). The samples for SEM were prepared by coating the powder with gold using the PVD method. The particle size was determined by applying the line intersection method on a scanning microphotograph with over 200 particles for each sample.

The nitrogen gas absorption BET method (Sorptomatic 1990, Thermoquest CE Instruments) was used for the determination of the specific surface areas of the silica powders. The samples (0.20–0.22 g) for absorption measurement were thoroughly degassed at 150 °C for 3 h. Knowing the absorbed volume of N_2 (purity 99.99%), specific surface areas of the silica powders were determined by applying the BET method (based on the correlation $p/(V_{ads}\ (p_0 - p))$ vs. p/p_0, where p_0 is the saturation pressure, p is the equilibrium pressure, V_{ads} is the absorbed volume of nitrogen). In addition, the Dubinin Radushkevich method (correlation log (V_{ads}) vs. $\log_2 (p_0/p)$ for the determination of the specific surface area was also used. The volume of the pores was evaluated using the Gurvich correlation, V_{ads} vs. p/p_o. The average and the maximum radius of the pores and the cumulative volume of all pores were determined using the Lecloux and Pirard method based on the Dollimore Heal pore-sizes standard absorption isotherm. The assumption that the synthesized particles were spheroids enabled the calculation of the average radius of the particles ($d_{BET} = 6/\rho S_w$), where S_w is the specific surface area and $\rho = 2.65$ g/cm^3 is the theoretical density of the synthesized silica powders.

3. Results and discussion

3.1. Structure and substructure of sol particles

3.1.1. Silica tetrahedral and infrared spectroscopy

Silica sol after drying: The IR spectrum of the silica sol dried at 150 °C exhibited band at 3380 cm^{-1}, which correspond to the extended vibration of the silanol group (Si-OH) (Fig. 1). The band of the twisting vibration of the OH^- group of molecular water is at 1584 cm^{-1} (usual literature value 1628 cm^{-1}). The band at 1329 cm^{-1} corresponds to the transversal and longitudinal asymmetric vibrations in rigid four-component siloxan rings-silica tetrahedrons, with the dominant participation of the

longitudinal vibration, while the band at 1061 cm^{-1} correspond to the transversal asymmetric Si-O-Si vibrations. Shifting of the wave number values to smaller values indicates the movement of O atoms along the direction parallel to the Si-Si axis, causing a distortion in adjacent Si-O bonds and the asymmetric transversal oscillations by the corresponding cation movement [22-27].

The oscillation at 920 cm^{-1} with a small shoulder indicates an extended Si-OH vibration. The vibrations at 747 cm^{-1} and 422 cm^{-1}, related to the rocking vibration deformations in Si-O-Si chains, are shifted toward smaller wave numbers due to the couplings of transversal symmetric vibrations of O atoms along the bisection line of the Si-O-Si angle, with the simultaneous movement of Si cations.

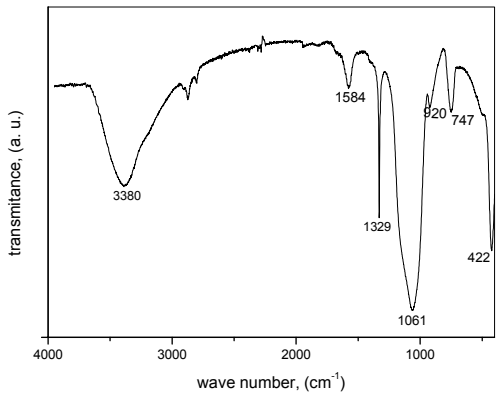

Fig.1. IR spectra for the sample of silica sol dried at 150 °C.

Silica powder after the spray pyrolysis process: All bands observed in the dried sols are also visible in the samples subjected to spray pyrolysis, although some of the bands are slightly shifted. The band corresponding to the vibration of silanol groups is shifted from 3380 cm^{-1} to 3387 cm^{-1}, while the band corresponding to the bending vibration of the OH^- group is at some place. The intensities of the bands corresponding to OH^- vibrations at 3387 cm^{-1} and 1557 cm^{-1} are slightly reduced (Fig. 2).

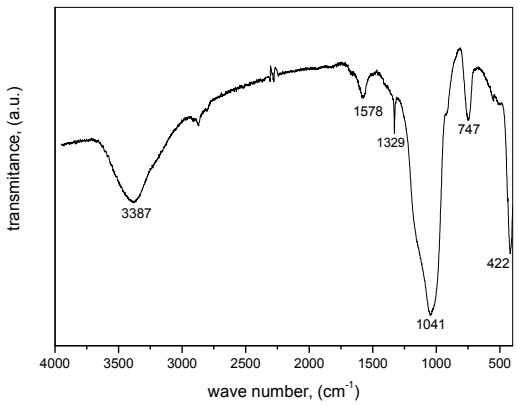

Fig. 2. IR spectra of the silica powder obtained by the spray pyrolysis process.

3.1.2. Self-assembled silica chains and thermo-chemical analysis

3.1.2.1. Thermochemical analysis of the SiO_2 powder

DT and TG analysis: The samples of the SiO_2 sol powder dried at 150 °C and then subjected to DT and TG analysis showed the first changes in mass in the temperature range between 20 °C and 110 °C (physically adsorbed bonded water), and the second changes in mass at in the temperature range from 360 °C to 595 °C or 630 °C (constitutional water), depending on the rate of heating (Figure 3). It can be seen that, depending on the rate of heating, the peak corresponding to the final dehydroxylation temperature of the silica sol moved from 560 °C up to 590 °C for powder heating rates of 5 °C/min and 10 °C/min, and from 600 °C up to 630 °C for powder heating rates of 20 °C/min, 30 °C/min and 50 °C/min. Also, for these powder heating rates, the final temperature of the elimination of adsorbed water from the system increased with increasing heating rate.

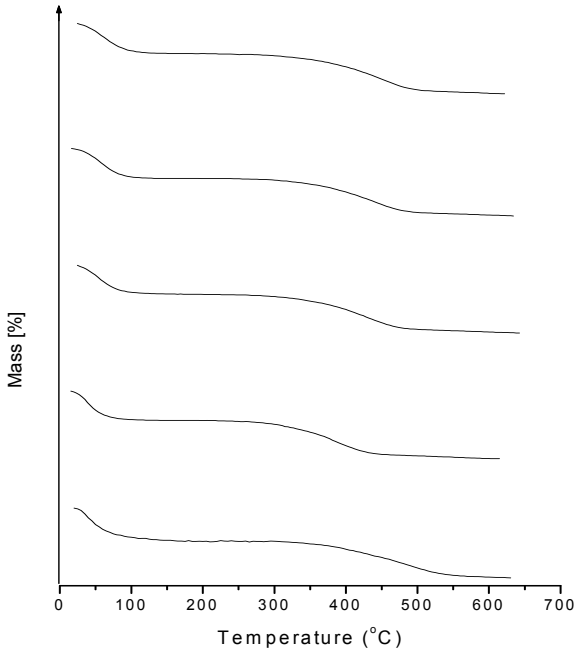

Fig. 3. The TG curves of the silica sol samples for different heating rates.

Considering the DTA curves shown in Figure 4, the endothermic peaks correspond to the water desorption processes, i.e., in the temperature range from 20 °C – 150 °C, physically adsorbed water and water adsorbed inside the nano-pores, and to constitutive water at the temperatures of 505 °C, 520 °C and 555 °C for the heating rates of 5 °C/min, 30 °C/min and 50 °C/min, respectively.

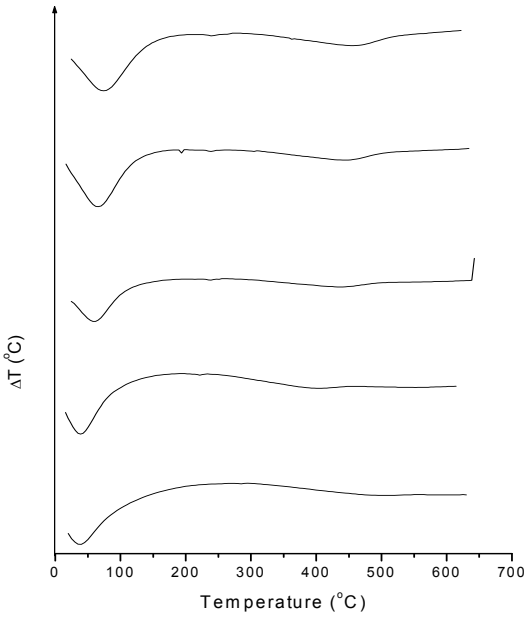

Fig. 4. The DT curves of the silica sol samples for different heating rates.

The mass losses and the endothermic changes in the system caused by heating may be related to elimination processes of adsorbed water at the surfaces of the particles and inside their nano-pores (temperatures from 20 °C – 150 °C), and to dehydroxylation processes, which commence at 340 °C – 360 °C and cease at 560 °C – 630 °C. Hence, it is probable that no further phase changes occur between 630 °C and 800 °C.

Activation energy of the dehydroxylation process of the silica sol: Taking into account the Arrhenius equation:

$$v = v_0 e^{\frac{-E_a}{RT}} \tag{1}$$

and

$$\frac{v_1}{v_2} = e^{-\frac{E_a}{R}\left(\frac{1}{T_1}-\frac{1}{T_2}\right)} \tag{2}$$

where v_1 and v_2 are the heating rates with the corresponding endothermic maximums T_1 and T_2 at which the dehydroxylation/dehydratation processes occur. Further more:

$$\ln\frac{v_1}{v_2} = -\frac{E_a}{R}\left(\frac{1}{T_1}-\frac{1}{T_2}\right) \tag{3}$$

Now, for each pair of values ln v_1/v_2 and corresponding values $1/T_1$ -$1/T_2$ in Figure 5, it is easy from the corresponding slope to evaluate the activation energy of the dehydroxylation process inside the given structural unit which defines the silica sol chain.

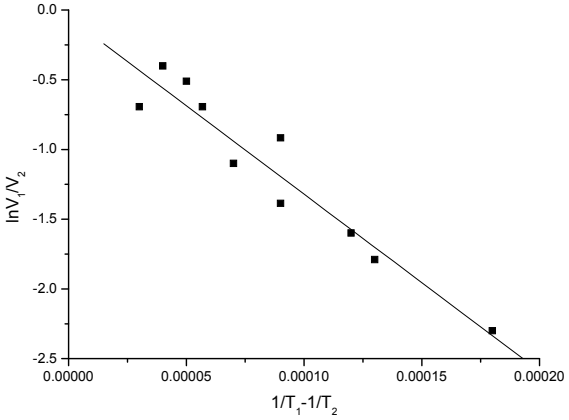

Fig. 5. The activation energy determined using Equation (3).

The activation energy determined for the dehydroxylation process of structural unit of the silica sol was 211 kJ/mol. From this value, it was possible to calculate the values of the activation energies for each OH group inside the structural unit of the silica sol; this value was 1.1 eV. Since in each dehydroxylation reaction, two OH groups are involved the necessary energy is 2.2 eV or 0.22 aJ (atto J).

3.1.2.2. Calculation of the basic structural unit of the silica sol

The TGA data enable the basic structural unit of the silica sol to be defined. Thus, the measured mass loss caused by heating (elimination of the constitutive water) during the dehydroxylation process lay between 3.02 and 3.47 %. Since during the very high rates of heating, in addition to the elimination of the constitutive water also some small quantities of water entrapped in the smallest nano-pores was registered, it is advisable to use the mass loss value registered during the lowest rate of heating., i.e., 3.02 %, for the calculation of the basic structural unit. Thus, it is possible to define the number of assembled silicon acid molecules during the formation of the given structural unit, as well as the number of residual Si^{4+} and O^{2-} ions which are together with an OH group inside a given unit. The theoretical mass loss in the dehydroxylation process of silicon acid during the formation of a given structural unit is 37.5 %, involving 2 OH^- and 2 H^+ ions (the mass of H^+ is much lower than that of OH^- and may be neglected). It is assumed that each silicate chain contains two OH^- groups, one at the beginning and one at the other end of the chain, now from the mass loss of 3.02 %, the calculated number of groups is 0.16 OH^- per silicon acid chain.

Considering the mentioned proposition, the mass of the average length of the overall silica chain, M_{SiO2}, is expressed by:

$$n\,M_{Si} + (2n-1)\,M_O + 2\,M_{OH} = M_{SiO2}\,, \qquad (1)$$

where M_{Si}, M_O and $M_{OH,}$ are the atomic masses of Si, O and OH, respectively. Furthermore:

$$\frac{2M_{OH}}{nM_{Si} + (2n-1)M_O + 2M_{OH}} = u_{OH}\,. \qquad (2)$$

Introducing the corresponding values of the atomic masses of all the constituent elements with the frequency of the smallest structural chain unit-silica tetrahedron and assuming that u_{OH} is equal to the heating loss $G_z = 0.03$, it is possible to calculate n and furthermore the number of SiO_2 tetrahedrons in a silica chain, as well as the complete chain structure.

From more precise calculations, the results show that about 40 % of the chains have 16 assembled Si atoms and about 60 % have 20 assembled Si atoms.

The basic structural unit of the silica chain consists of silica tetrahedrons which are interconnected at their corners by oxygen atoms. At the opposing chain ends, two OH^- groups are positioned at the end corners.

Prediction of the configuration of the particular chains as well as the manner of packing is not an easy task. Since the chains are very long and their basic units (tetrahedrons) may be positioned in many different ways, depending on the curvature angles between the silicon and oxygen atoms (in particular at the top corners), the forms in which the silica sol particles have the smallest surface free energy are realized during the self-assembling process.

Assuming a linear and extended chain, what is an unrealistic case, the length of the chain could be between 4.8 nm and 6.1 nm. Furthermore, the largest chain diameter (tetrahedron base) could be 0.14 nm (the length of the baseline). In accordance, the chain volume could be between 0.073 nm^3 and 0.092 nm^3.

Finally, assuming a more realistic case, i.e., spherical or spheroid chain forms, the SiO_2 chains could have a diameters between 0.5 nm and 1 nm, depending on the form regularity (ellipsoid eccentricity). Such forms could be easily assembled in similar forms at the sol particle level (spherical shape, as was shown from TEM measurements).

3.3. Silica sol particles: transmission electron microscopy and dynamic light scattering

The particle size of silica sol was determined using transmission electron microscopy.

The microphotograph (Fig. 6.) shows that the sizes of the silica particles are between 5 and 10 nm, while their shape is mostly spherical, representing agglomerates of finer particles. At the particle edge, contours of smaller particles can be observed. The mean size of these small particles is 7.5 nm.

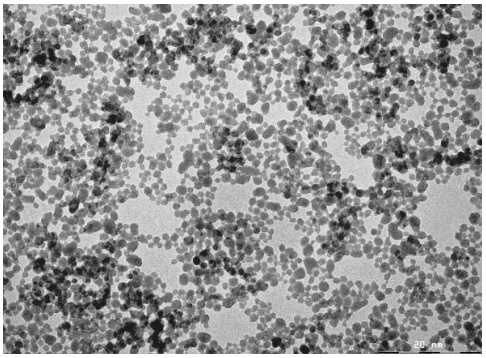

Fig. 6. The size and morphology of the silica sol particles.

In addition to the TEM method, the size distribution of the silica sol was determined using the dynamic light scattering method (quasi-elastic light scattering). The particle size distributions were calculated from the measured data using built-in instrument size software and the obtained results are shown in Table 1.

Table 1. The particle size distribution of the SiO_2 sol determined by dynamic light scattering

d, nm	Partition, %	d, nm	Partition, %
<4.5	0	13.8	0
5.1	0	15.6	0
5.9	0	18.5	0
6.5	0	20.8	0
7.6	98	23.9	0
8.8	0	27.8	1
10.4	0	32.3	1
11.7	0	>35	0

The obtained data show a very narrow size distribution of the silica sol particles: 98% of all particles have a diameter of 7.7 ± 0.5 nm, while the remaining 2% were agglomerates.

3.4. Structure design: particles and sub-particles and SEM

A typical distribution of the diameters of the SiO_2 particles and the fractional amounts are shown in Fig. 7 and Table 2, respectively.

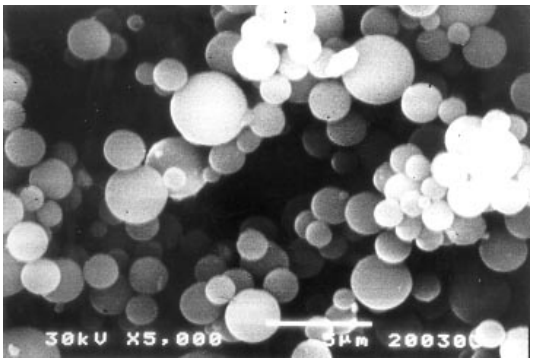

Fig. 7: SEM. A typical distribution of the sizes of the SiO_2 particles obtained by the spray pyrolysis process.

The mean diameter of the SiO_2 particle, d_{ap}, can be obtained using the equation:

$$d_{ap} = \frac{\Sigma_{i=1}^{n} n_i d_i}{\Sigma_{i=1}^{n} n_i} \quad (3)$$

where n_i is the fraction of particles having diameter d_i. The fractions of particles of a given diameter were experimentally determined from SEM microphotograph showing more than 200 particles. The calculated mean diameter of the SiO_2 particles was 1.68 μm

Table 2. The size distribution of the experimentally obtained particles

d_p,μm	1	1.24	1.53	1.78	2.47	3.48
Partition	0.03	0.20	0.36	0.25	0.14	0.02

A similar approach can be used for the theoretical prediction of the size of the droplets and particles using equations (A4) and (A5). Equations (A6) and (A7) were employed for the determination of the fractional amounts of their sizes [14, 17]. Also, in agreement with this model, the sizes of the aerosol droplets were in the range 3.6 μm - 7.5 μm (Table 3, row 1) and the average droplet diameter was 4.14 μm. It is obvious, from the theoretical model that the shift of diameter values in this interval is the consequence of the deformation of the 3D capillary standing waves formed on the surface of the precursor liquid column under the action of the given ultrasonic field.

Table 3. The characteristic parameters of the theoretically predicted particle size distribution

d_d,μm	3.6	5.57	7.5
Participation	0.32	0.45	0.23
f,MHz	2,37	1,23	0,79
Δf,MHz	0,67	0,47	0,91
d_p,μm	1,22	1,89	2,55

Applying equation (A5), the values of particle diameters were between 1.24 μm and 2.47 μm (Table 3, row 5), which corresponds to the changes of forced frequencies of the applied ultrasonic field (caused by damping factor of ultrasonic wave, in agreement with the theoretical model) from 2.37 to 0.79 MHz (Table 3, row 3).

The average SiO_2 particle diameter (1.83 μm) obtained by applying Eq. (2A), (4A), and (6A) and (7A) shows fairly good agreement with the experimentally obtained values (1.71 μm).

It is obvious, that in both cases, the distributions were similar and narrow, i.e., 92.5 % of all the measured and theoretically estimated diameters were within the size interval 1.25 – 2.5 μm, see row 5 in Table 3

Furthermore, the model allows the estimation of other characteristic parameters of the synthesis of SiO_2 powder, such as the actual shifted frequency of the formation of droplets and the difference between this frequency and the forced frequency of the applied ultrasonic field generator (Table 3, rows 3 and 4).

From Fig. 8, it can be seen that each particle has a complex substructure, which is composed of numerous sub-particles. From the experimental data, the diameters of these sub-particles were between 25 and 30 nm.

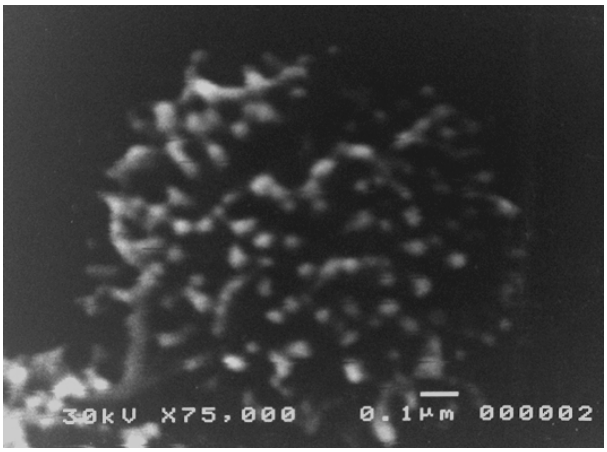

a

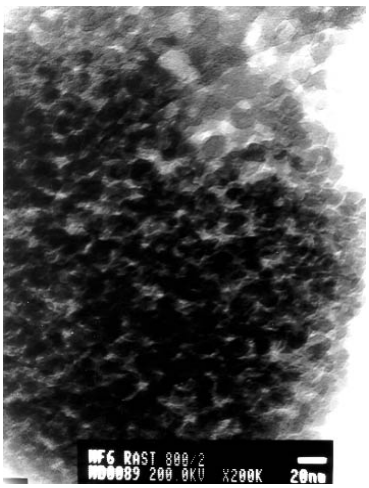

b

Fig. 8. A typical sub-structure of the SiO_2 particles obtained by the spray pyrolysis process.

In accordance with this theoretical model of the design of substructure particles, the average sub-droplet size (d_{sd}) can be calculated from equation (A10) and the average diameter of the sub-particles (d_{sp}) can be calculated using equation (A5). These values are d_{sd}=128 nm and d_{sp}=38.4 nm, respectively

Therefore, the entire particle structure is designed in 5 levels: (i) particles with a mean diameter of 1.8 μm, (ii) sub-particles with a mean diameter of 38.4 nm; (iii) sol particles with a mean diameter of 7.5 nm, (iv) sub-nano-sized silicate chains-motives consisting of silica tetrahedrons and (v) silica tetrahedrons which define the organization of the system at the shortest distances. The

number of tetrahedrons in an average silica chain-motive is 18.

Hence, under conditions when it is possible to neglect the interaction of particles, it seems that it is possible to retain the structure and properties of a given system at each individual level. The calculations related to each structural level and the values measured (up to the highest-particle level) show that a SiO_2 particle can be composed of a series of build up entities belonging to different levels of its structural hierarchy.

Experimental results related to previous investigations of the average particle sizes (d_p) and the distributions thereof (I) for various volume precipitated systems, such as Al_2O_3, TiO_2, hydroxyapatite-CHA, mullite, and cordierite) [11, 12, 14, 15, 17] (shown in Table 4), enabled a comparison of them with the corresponding results for the SiO_2 system. From these data, it can be noticed that the particles of each system presented in Table 4, as for the SiO_2 system, were always concentrated around one value of the diameter. In general, it can be concluded that the largest number of particles had a relatively narrow size distribution range and approximately 80% of particles had a diameter very close to the average diameter.

Table 4. The average particle sizes and size distributions for some previously synthesized systems.

	Al_2O_3 [11,12]	d_p [μm]	0.2	0.3	0.39	0.47	0.56	0.65	**0.74**	0.82	0.91
		I	0.02	0.02	0.03	0.16	0.21	0.24	0.12	0.17	0.08
	CHA [15,17]	d_p [μm]	0.41	0.5	**0.55**	0.61	0.65	0.71	0.81	0.91	
		I	0.08	0.21	0.32	0.21	0.2	0.11	0.02	0.03	
	Mullite [12, 17]	d_p [μm]	0.3	0.52	0.7	**0.91**	1.19	1.3	1.52	1.7	
		I	0.02	0.08	0.28	0.10	0.15	0.03	0.06	0.01	
	Cordierite [12, 17]	d_p [μm]	0.4	0.5	0.6	0.7	**0.8**	**1.2**	1.4		
		I	0.08	0.04	0.3	0.37	0.19	0.04	0.04		

In addition to the comparative analysis of the experimental data, the particle diameters for various previously investigated systems were theoretically calculated using the diameters of the aerosol droplets, estimated by the in the literature most frequently used Lange equation [25] and by using the V. Jokanovic model [11-18], as well as the equations defining the reduction of the size of the droplets during their consolidation [27], (given in Table 5). The agreement of these data with the data obtained for the above discussed SiO_2 system, as can be noticed from Table 5, is evident.

As can be seen in Table 5, the experimental values for these systems, as the SiO_2 system, show a high level of accordance with the given theoretical calculations, with deviations usually less than 10%. The sign "+" sign denotes a higher value compared to the experimental one, whereas the "–" sign denotes a lower value compared to the experimental one.

Table 5: The experimentally and theoretically calculated average diameters for some previously synthesized particles.

System	d_L [μm]	d_V [μm]	d_{exp} [μm]	d_{exp}-d_v [%]
Al_2O_3 [11, 12]	0.53	0.77	0.73	+5.2
CHA [15,17]	0.39	0.56	0.57	-1.8
Mullite [12,17]	0.60	0.89	0.94	-5.6
Cordierite [12,17]	0.72	1.06	0.91	+14.2

The similar case is present from the From the morphological point of view, the SiO_2 system is very similar to the other volume precipitated systems presented here. Most frequently spherical forms are preferred, with an evident substructure (comprising smaller particles of the sub-particles of the system, packed within a given particle and showing their characteristic sub-design).

3.5. Sub-particle design and BET analysis

Comparing the results of the specific surface area determination (BET method: d_{BET} = 27.4 nm, see Table 6) with results of SEM (d_{sp}= 25-30 nm), including the theoretical predictions of them by the model of the break-

up of capillary waves presented in this paper (d_{sp}= 38.4 nm), it is clear that the SiO_2 particles are agglomerates of small SiO_2 sub-particles of size between 25 and 30 nm. In addition, it is evident that the average diameter of the pores of the SiO_2 particles of 11 nm as measured by the BET method agrees well with the expected voids between the sub-particles inside the primary SiO_2 particles. A similar compliance was found for the pore volume per unit mass.

This is additional evidence of the agreement between the corresponding measurements by the SEM and BET method (Fig. 8. and Table 6.) and the results estimated using the presented theoretical model for the size distribution of the sub particle (Table. 4).

Table 6. Characteristic geometric parameters of the silica powders obtained by analysis of nitrogen absorption isotherms.

Specific area, m^2/g	$d_{BET(p)}$, nm	d_{pore}, nm	V_{pore}, cm^3/g
67.5	27.4	11	0.153

4. Conclusions

The synthesis of SiO_2 particles using spray pyrolysis in combination with the hydrothermal method of silica sol synthesis was discussed. The structural design of the silica particles at different structural levels was investigated from i) the primary particle level, ii) the sub-particles level, iii) the sol level, iv) the chain level and v) the silica tetrahedron level. The silica chain size was determined using TGA analysis.

According to SEM and BET measurements, the mean particle size was 1.71 μm, the sub- particle size was 25-30 nm, while the corresponding values, obtained on the basis of the applied theoretical model, were 1.8 μm and 38.4 nm, respectively. The average diameter of the sol particles was 7.5 nm (TEM, dynamic light scattering) and the size of the structural motive of the silicon dioxide chain was 18 cells. The silicon dioxide tetrahedron (IR spectroscopy) is the basic structural unit of a silica chain.

Calculations based on the presented theoretical model show fairly good agreement with experimental results at both the particle and the sub-particle level, which confirms its applicability to this system.

Acknowledgement

We wish to acknowledge the support of the Ministry of Science of the Republic of Serbia.

References

[1] S. W. Kang, Y. S. Kim, J. Korean Inst. Met. Mater. **34**, 1375 (1996).
[2] B. Jokanović, T. Damjanović, R. Weiss, G. Borchardt, Mat. Sci. Forum, **453-454**, 329 (2004).
[3] W. H. Suh, K. S. Suslik, J. Am. Chem. Soc., **127**, 12007 (2005).
[4] H. Sertchook, D. Avnir, Chem. Mater. **15**, 1690 (2003).
[5] D. Hreniak, E. Zych, L. Kepinski, W. Strek, J. Phys. Chem. Solids, **64**, 111 (2003).
[6] A. Lempicki, A. J. Wojtowich, C. Brecher, in: S. R. Rotman (Ed.), Wide-gap luminescent materials: Theory and applications, Kluwer, MA, 1996.
[7] R. Bertoncello, L. Milanese, R. Negro, L. Saragoni, S. Barison, J. Non-Cryst. Solids **324**, 73 (2003).
[8] Y. Fukada, P. S. Nicholson, J. Eur. Cer. Soc. **24**, 17 (2004).
[9] M. Morita, D. Rau, S. Kajyama, T. Sakurai, M. Baba, M. Iwamura, Mat. Sci-Poland, **22**, 5 (2004).
[10] O. D. Velev, T. A. Jede, R. F. Lobo, A. M. Lenhoff, Nature, **389**, 447 (1997).
[11] V. Jokanović, Dj. Janaćković, A. M. Spasić, D Uskoković, Mat. Trans., JIM **37**, 627 (1996).
[12] V. Jokanović, Dj. Janaćković, D. Uskoković, Ultrason. Sonochem. **6**, 157 (1999).
[13] V. Jokanović, Dj. Janaćković, D. Uskoković, Nanostruct. Mater. **12**, 349 (1999).
[14] V. Jokanović, A. M. Spasić, D. Uskoković, J. Coll. Interf. Sci., **278**, 342 (2004).
[15] V. Jokanović, I. Nikčević, B. Dačić, D. Uskoković, J. Cer. Proc. Res., **5**, 157 (2004).
[16] V. Jokanović, D. Uskoković, Mat. Trans., JIM, 228 (2005).
[17] V. Jokanović, "Structures and substructures in spray pyrolysis process: “Nanodesigning", in Finely dispersed particles: micro-, nano- and ato-engineeering, Ed. A. M. Spasic and J. P. Hsu, CRC Press, Taylor and Francis, (2005).
[18] V. Jokanovic, U. B. Mioc, Z. Nedic, Solid. State Ionics **176**, 2955 (2005).
[19] E. Matijevic, Chem. Mater. **5**, 412 (1993), -426.
[20] A. van Blaaden, A. Vrij, Langmuir, **8**, 2921 (1992)
[21] H. Zhu, Y. Ma, Y. Fan, J. Shen, Thin Sol. Films **397**, 95 (2001).
[22] F. Geotti-Bianchini, M. Preo, M. Guglielmi, C. G. Pantano, J. Non-Cryst. Solids **321**, 110 (2003).
[23] D. R. Daughton, J. MacDonald, N. Mulders, J. Non-Cryst. Solids **319**, 297 (2003).
[24] P. Innocenzi, J. Non-Cryst. Solids **316**, 309 (2003).
[25] R. J. Lang, J. Acoust. Soc. Am. **34**, 6 (1962).
[26] R. L. Peskin, R. J. Raco, J. Acoust. Soc. Am, **35**, 1378 (1963).
[27] G. V. Jayan, S. C. Zhang, G. L. Messing, J. Aerosol. Sci. Technol., **19**, 478 (1993).
[28] A. Bose, R. K. Gilpin, M. Jaroniec, J. Coll. Interf. Sci., **240**, 224 (2001).

Appendix

7A1. Theoretical model for designing the structure of a secondary particle

The waves formed by transferring ultrasound oscillations in a given precursor, depending on the superposition conditions, have a complex spatial form that primarily depends on the muting factors of the oscillation in different directions (in the direction of deformation or in the direction perpendicular to this direction) and the given frequency of the ultrasonic generator [11,12,14,17]. For small thicknesses of liquid columns, the difference in the muting factor of the transversal and longitudinal waves is insignificant, and in this case (in the process of compulsory ultrasound excitation), standing waves with a spherical form are obtained [11,12,14,17]. Based on the 3D model of capillary standing waves formed at the surface of the meniscus, the following expression is obtained by analyzing the harmonic potential rate function of the created disturbance [11,12,14,17]:

$$\frac{\partial \varphi}{\partial t} + g\xi - \frac{\sigma}{\rho}\left[\frac{\partial^2 \xi}{\partial x^2} + \frac{\partial^2 \xi}{\partial z^2}\right] = 0 \quad , \tag{A1}$$

where φ is the potential rate of the capillary standing waves, σ is the surface tension of the solution, g is the inertial force acting on the liquid in contact with the ultrasonic oscillator, ξ is the amplitude of the formed standing wave, x and z are coordinates equivalent to the given amplitude and t is the time.

The final solution of equation (A1) can be written in the following form [30-35]:

$$d = \left(\frac{\pi\sigma}{\rho f^2}\right)^{\frac{1}{3}}, \tag{A2}$$

where d is the mean radius of the formed aerosol droplet, ρ is the density of the solution, and f is the excitation frequency of the given ultrasonic oscillator.

If it is assumed that the difference in the muting factor of transversal and longitudinal waves is not insignificant when the thickness of the liquid column is not insignificant, then it is possible to present the standing capillary wave in the form of a Laplace equation expressed in polar coordinates [11,12,14,17]:

$$\rho \frac{\partial^2 \varphi}{\partial t^2}_{r=R} - \frac{\sigma}{R^2}\left\{2\frac{\partial \varphi}{\partial r} + \frac{\partial}{\partial r}\left[\frac{1}{\sin\theta}\frac{\partial\left(\sin\theta \frac{\partial \varphi}{\partial \theta}\right)}{\partial \theta} + \frac{1}{\sin^2\theta}\frac{\partial^2 \varphi}{\partial \varepsilon^2}\right]\right\} = 0, \tag{A3}$$

where r is the radius of the aerosol droplet, ε and θ are angles corresponding to the equation transformed into polar coordinates.

The solution of this equation gives a set of solutions corresponding to possible discrete values of the radiuses of aerosol droplets equivalent to the given muting factor of the excited capillary waves in a given liquid column:

$$d = \frac{1}{\pi}\left(\frac{2\sigma\pi}{\rho f^2}\right)^{\frac{1}{3}}\left[l(l-1)(l+2)\right]^{\frac{1}{3}}, \tag{A4}$$

The values of the diameter of particles formed from aerosol droplets through solidification of the aerosol droplets are calculated using the equation [11,12,14,17,27]:

$$d_p = d_d\left(\frac{c_{pr} M_p}{\rho_p M_{pr}}\right)^{\frac{1}{3}} \tag{A5}$$

where d_p is the diameter of the powder particle, ρ_p is the density of the powder particle, M_p is the molecular mass of the powder, c_{pr} is the concentration of the precursor (solution used for spraying) and M_{pr} is the molecular mass of the precursor.

The particle size distribution can be estimated from the equation [12,14,17]:

$$I_1 : I_2 : \ldots : I_N = \frac{1}{\Delta f_1} : \frac{1}{\Delta f_2} : \ldots : \frac{1}{\Delta f_n} \tag{A6}$$

where I_1, I_2, I_N are the intensities (participation) of the appearance of corresponding discrete values of the particle diameters in a given spectra, or the corresponding numerical values defining the appearance frequency of a given discrete value. Furthermore, Δf_1, $\Delta f_2, \ldots$, Δf_n are the displacements of the real frequencies from the forced frequency of the ultrasonic oscillator caused by the damping factor of the precursor liquid column. The relative ratios of the intensity (the frequency of a particular particle diameter), if normalized, provides the basic relationship for the calculation of the absolute value for the intensity [12,14,17]:

$$I_1 + I_2 + \ldots + I_N = 1 \tag{A7}$$

7A2. Theoretical modeling of the sub-structure of a powder particle

The radius of nanoelements; nanodroplets and nanoparticles which form the given substructure of an aerosol droplet, i.e., the secondary particles formed by its solidification, can be determined using the wave equation of a centrally symmetric standing wave formed as the result of transferred excitation of the ultrasonic generator to the droplet itself, and can be presented by [12-14,17]:

$$\frac{\partial^2 \varphi}{\partial t^2} = c^2 \frac{1}{r^2}\frac{\partial}{\partial r}\left(r^2 \frac{\partial \varphi}{\partial r}\right), \tag{A8}$$

where c is the spreading rate of the disturbance and r is the radius of the aerosol droplet.

Based on the derivation given in detail previously [12,14], the following solution of the equation is obtained [12-14, 17]:

$$\mathrm{tg}\, kr = kr, \tag{A9}$$

where k is the wave number ($k = \frac{2\pi f}{c}$), numerical solution of which is given by the set [12-14,17]:

$$r = \frac{Nc}{f}\ , \tag{A10}$$

where N is a numerical constant that has different values for different solutions (values of the numerical constant) as a set of solutions of equation (A5). These values are given as 0.175; 1.21; 1.72; 2.23; 2.74; 3.82; ... and they depend on the form of sub-structural elements comprising the particle formed in the aerosol droplet and sub-droplet during the solidification process.

*Corresponding author: vukomanj@ptt.yu
vukomanj@beotel.net